ADVANCED FUNCTIONAL MATERIALS
www.afm-journal.de

Self-Powered Distributed Water Level Sensors Based on Liquid–Solid Triboelectric Nanogenerators for Ship Draft Detecting

Xiangqian Zhang, Min Yu, Ziran Ma, Han Ouyang, Yang Zou, Steven L. Zhang, Hukai Niu, Xinxiang Pan, Minyi Xu, Zhou Li,* and Zhong Lin Wang**

Ship draft measurement is of great significance for ensuring navigation safety and facilitating ship control. In this work, a self-powered water level sensor based on a liquid–solid tubular triboelectric nanogenerator (LST-TENG) is proposed and analyzed. The LST-TENG is made of multiple copper electrodes uniformly distributed along a polytetrafluoroethylene (PTFE) tube. When water flows into the PTFE tube, it induces alternating flows of electrons between the main electrode and the distributed bottom electrodes. The obvious peaks in the derivative of open-circuit voltage with respect to time are found to correspond with the electrode distribution. Then it can be utilized as a robust and sensitive indicator for detecting the water level as the number of obvious peaks in the derivative of open-circuit voltage is directly related to the water level height. The ship draft is successfully detected using the LST-TENG with an accuracy of 10 mm. It shows that the water level sensor has stable performance for liquid–solid interface monitoring. Therefore, this LST-TENG is self-powered, robust, and accurate for extensive applications in marine industry.

1. Introduction

The ship draft, the vertical distance between the waterline and the bottom of the hull, could be used to effectively determine the weight of loaded or discharged cargo on the ship. The real-time detection of the draft is also significant for reducing the ship grounding or other security incidents and protecting the channel safety.[1] At present, the main methods to obtain ship's draft includes visual observation, ultrasonic ranging, and pressure and photoelectric sensing.[2] By visual observation, the measurement of ship draft is roughly estimated though manually reading the markings on the side of the ship. However, a downside of using visual observation is that it is difficult for a user to perform readings during adverse conditions such as rough seas, fog, storms, etc. Ultrasonic technique is used to measure the distance between the deck and the water surface, while the influence of the temperature and humidity is significant. The problems in installation and maintenance cause that the pressure and photoelectric sensors to be rarely used in practice.[2] Thus, it is necessary to design an efficient and robust method to convert dynamic water level into digital information.[2,3]

Recently, a class of self-powered sensors based on triboelectric nanogenerator (TENG) were introduced by converting mechanical motion into electrical output signal.[4–8] On the basis of a coupling effect between triboelectrification and electrostatic induction, TENGs have been utilized for energy harvesting,[9–17] chemicals detecting,[18–20] health monitoring,[21–23] pressure, spatial displacement, and liquid/gas flow sensing,[24–34] and surface antifouling.[35,36] Recently, Zhu and co-workers[37] designed a single-electrode-based triboelectric sensor array for detecting object motion inside of a plastic tube. A linear array of copper electrodes aligned along the tubing enables detection of location and speed of the steel ball inside. Based on the capillary and the triboelectrification effects on the liquid/solid interface, Hu and co-workers[38] developed

X. Zhang, Z. Ma, H. Niu, Prof. X. Pan, Dr. M. Xu
Marine Engineering College
Dalian Maritime University
Dalian 116026, China
E-mail: xuminyi@dlmu.edu.cn
Dr. M. Yu, H. Ouyang, Y. Zou, Prof. Z. Li, Prof. Z. L. Wang
CAS Center for Excellence in Nanoscience
Beijing Key Laboratory of Micro-nano Energy and Sensor
Beijing Institute of Nanoenergy and Nanosystems Chinese Academy of Sciences
Beijing 100083, China
E-mail: zli@binn.cas.cn; zhong.wang@mse.gatech.edu
The ORCID identification number(s) for the author(s) of this article can be found under https://doi.org/10.1002/adfm.201900327.
S. L. Zhang, Prof. Z. L. Wang
School of Materials Science and Engineering
Georgia Institute of Technology
Atlanta, GA 30332-0245, USA
Prof. X. Pan
School of Electronics and Information Technology
Guangdong Ocean University
Zhanjiang 524088, China
Prof. Z. L. Wang
College of Nanoscience and Technology
University of Chinese Academy of Sciences
Beijing 100049, China

DOI: 10.1002/adfm.201900327

a triboelectric microfluidic sensor by utilizing the signals produced from the droplet/bubble for real-time liquid and gas flow detection. Zhang et al.[25] proposed a newly U-shaped TENG based on liquid–solid triboelectrification and Pascal's law. Xu et al. recently designed a highly sensitive wave sensor based on liquid–solid interfacing triboelectric nanogenerator.[24] Therefore, the TENG has a great potential application for a real-time water level monitoring system.

In this work, a novel water level sensor based on liquid–solid tubular triboelectric (LST-TENG) is designed and investigated. The LST-TENG is made of an independent main copper electrode and other multiple copper electrodes uniformly distributed along a polytetrafluoroethylene (PTFE) tube. When water flows into the PTFE tube, it induces alternating flows of electrons between the main electrode and the distributed bottom electrodes. The electric signal can be detected easily with dozens of volts generated by water moving. Especially, it is found that obvious peaks in the derivative of open-circuit voltage with respect to time are in correspondence with electrode distribution. Then it could be utilized as a robust and sensitive indicator for detecting the water level. In our investigation, this LST-TENG is verified to measure the water level information accurately and quickly for ship dynamic draft monitoring, with a accuracy of 10 mm, which is ten times higher than that of the traditional draft mark on the ship. Therefore, this self-powered water level sensor based on the LST-TENG has great industrial application in liquid–solid interface monitoring for marine field.

2. Results and Discussion

2.1. Structure and Working Principle of LST-TENG

Figure 1 shows the schematic diagram and working principle of the LST-TENG. A top copper electrode and multiple bottom electrodes were wrapped uniformly outside the surface of a PTFE tube to form a distributed-electrode tubular structure, as shown in Figure 1a,b. In addition, the LST-TENG is placed into an acrylic tube with a larger diameter to isolate water from electrodes, such as for the electrodes to avoid corrosion from seawater. Also, the air gap between the PTFE tube and the water could also reduce the effect of shielding from the water.[23] As water flows in the tube, induced charges transfer between the main electrode and distributed electrodes. PTFE is used as an electrification contact material due to its strong adsorption capacity for electrons. Figure 1c illustrates the working principle of the LST-TENG, which is similar to the solid–liquid freestanding TENG.[39] At the original position, PTFE selectively attracts electrons causing negative charges on the surface when water flows into PTFE tube for the first time. This phenomenon is governed by selective ion absorption.[39,40]

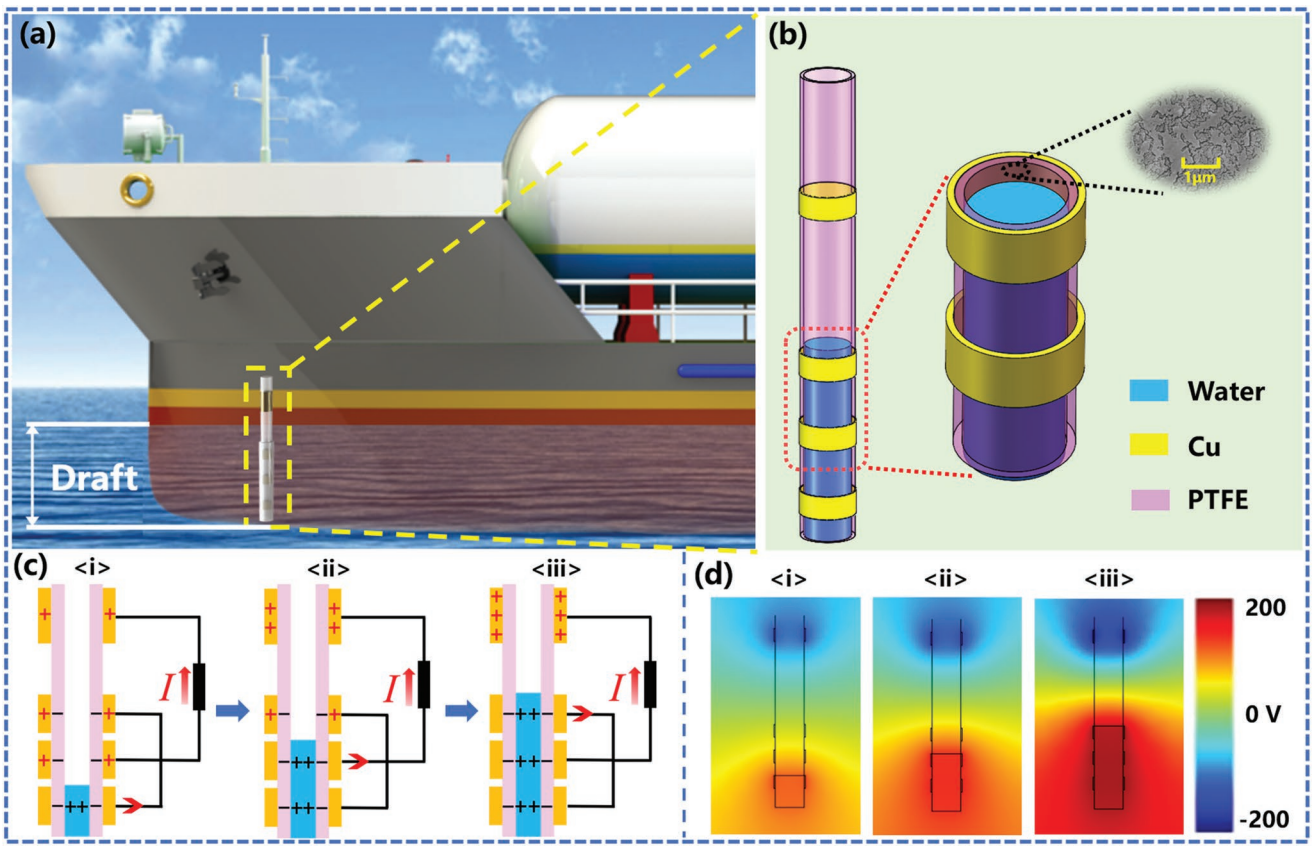

Figure 1. Structure and working principle of the liquid–solid tubular triboelectric nanogenerator (LST-TENG). Schematic diagram of the fabricated LST-TENG a) for ship draft measurement and b) its structure. Inset: SEM image of the PTFE inner surface. c) Working principle of the LST-TENG. d) Finite-element simulation of the voltage potential distribution of the LST-TENG under different water level.

Before the water enters the tube, the electrode is under an electrostatic equilibrium state. When water flows into the tube and destroy the electrostatic equilibrium, the water layer near the inner wall of the tube is positively charged. The nonstatic equilibrium induces a potential difference between the top electrode and the bottom distributed-electrodes, resulting in electrons transferring between the top electrode and the bottom electrodes (Figure 1c). The COMSOL Multiphysics software based on finite-element simulation is employed to calculate the potential distribution across the main electrode and distributed electrodes at different states, as shown in Figure 1d. The potential contour clearly shows that the potential difference between the two types of electrodes, which drives the current flowing in the external circuit.

The TENG can be treated as an ideal voltage source and a TENG's internal capacitor in series, thus the differential equation for the TENG unit with an external pure resistance R is as follows[4]

$$R\frac{dQ}{dt} = -\frac{1}{C}Q + V_{oc} \tag{1}$$

Here, V_{oc} is the open-circuit voltage, C is the TENG's internal capacitance, and Q is the transferred charge, respectively. For the LST-TENG with multiple bottom electrodes, the open-circuit voltage V_{oc} gradually increases when the water level rises from the bottom to a certain position, and it can be determined as follows

$$V_{OC} = V_{OC_e} + V_{OC_b} = \sum_i V^i_{OC_e} + \sum_j V^j_{OC_b} \tag{2}$$

Here, $V^i_{OC_e}$ is the induced voltage for water flowing over the ith bottom electrode region, and $V^j_{OC_b}$ is the induced voltage for water flowing over the jth blank region between a pair of neighboring bottom electrodes. The different performance of the output voltage $V^i_{OC_e}$ and $V^j_{OC_b}$ is investigated and utilized for identifying the water level in the following part.

2.2. Performance of LST-TENG

To characterize the performance of the LST-TENG, we measured the electrical output between the top electrode and the two bottom electrodes during water rises/falls in the tube, as shown in **Figure 2**. The water level in the tube was controlled by a linear motor to drive a syringe (Figure 2a). The two bottom electrodes labeled by **E1** and **E2**, respectively, were stacked to the outside surface of the PTFE tube. The height of the blank region (**B1**) between **E1** and **E2** is 50 mm, and the height of each electrode is 10 mm. Figure 2b shows the diagram of the water level at different electrode region and blank region.

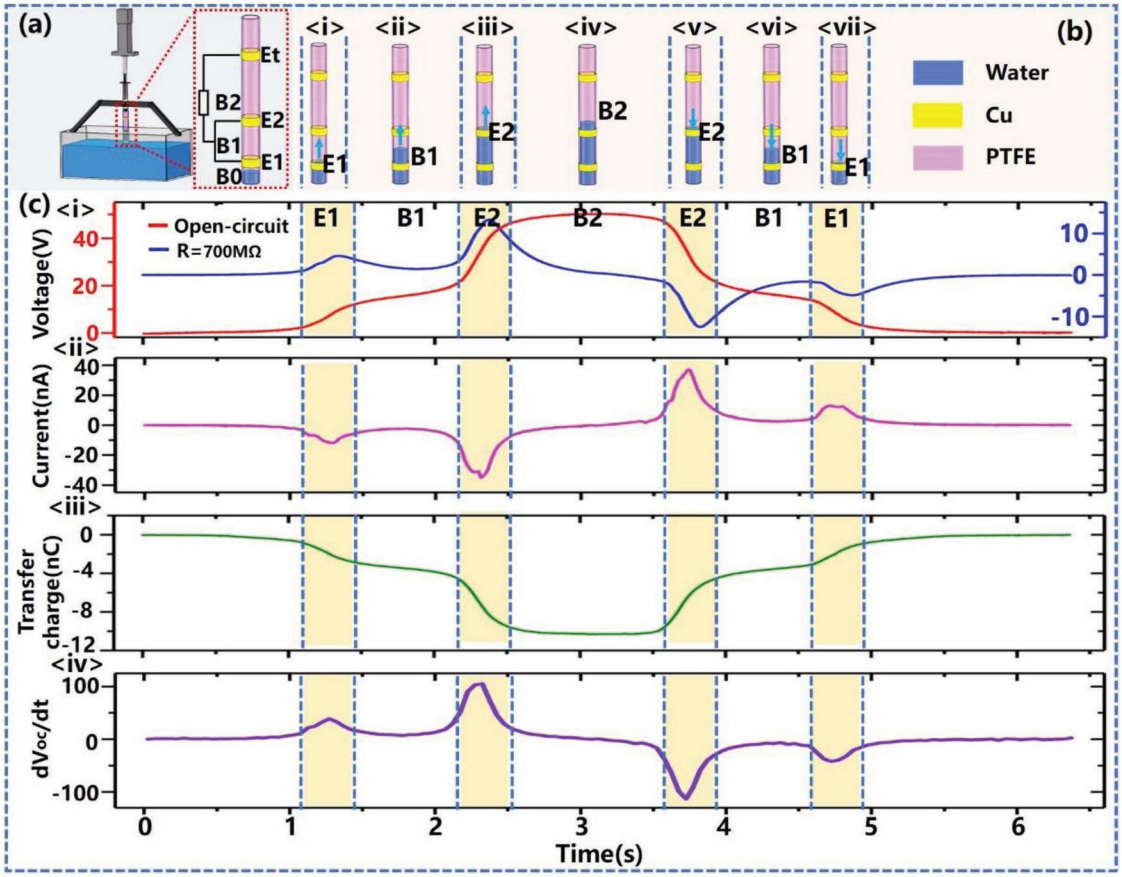

Figure 2. The electrical signal performance of the LST-TENG with a pair of bottom electrodes (**E1** and **E2**). a) The setup of water level controlling system. b) The process of water level increasing and falling. c) (i) The open-circuit voltage (V_{OC}) and the voltage (V_R) across a resistance of 700 MΩ, (ii) the short-circuit current (I_{SC}), (iii) the transferred charge (Q_{tr}), and (iv) the differentiating signals of the open-circuit voltage output (dV_{OC}/dt) during the water level rising above the electrode **E2** and falling below the electrode **E1**.

The electrical output between the top electrode (**Et**) and the bottom electrodes (**E1** and **E2**) were measured and compared during the water level rising above the electrode **E2** and falling below the electrode **E1**, as shown in Figure 2c. It is worth to note that the sensor could be fabricated long enough to prevent water reaching to the top electrode Et. When the water level rises across the bottom electrodes, there are peaks in the voltage signal across a resistance of 700 MΩ (Figure 2c(i)) and the short-circuit current signal (Figure 2c(ii)) of the LST-TENG. These peaks relate to the variation of the open-circuit voltage (Figure 2c(i)) and transferred charge (Figure 2c(iii)) with the water level moving within the electrode region and blank region, alternately. As shown in Figure 2c(i),(iii), the induced open-circuit voltage and transferred charge increases or decreases faster within the electrode region (**E1** and **E2**) than that in the blank region (**B1** and **B2**). Therefore, the growth rate of V_{OC_e} is greater than that of V_{OC_b}. To characterize the growth rate of the induced voltage, the derivative of open-circuit voltage signal respect to time is obtained. In the signals of dV_{OC}/dt, there is an obvious positive peak appearing in both **E1** and **E2** electrode region when water flows from the bottom to the **B2** area, as shown in Figure 2c(iv). Conversely, when the water level decreases, the value of dV_{OC}/dt becomes negative due to the voltage gradually decreasing, and a negative valley exists in the **E1** and **E2** electrode. Therefore, these obvious peaks, which are caused by the two different voltage variation modes of the LST-TENG, has great advantage as a robust and sensitive indicator for identifying the water level.

To improve the accuracy of the LST-TENG, the LST-TENGs with narrower blank region and multiple bottom electrodes were designed and investigated. **Figure 3**a,e shows the diagram of an LST-TENG with two and four bottom electrodes,

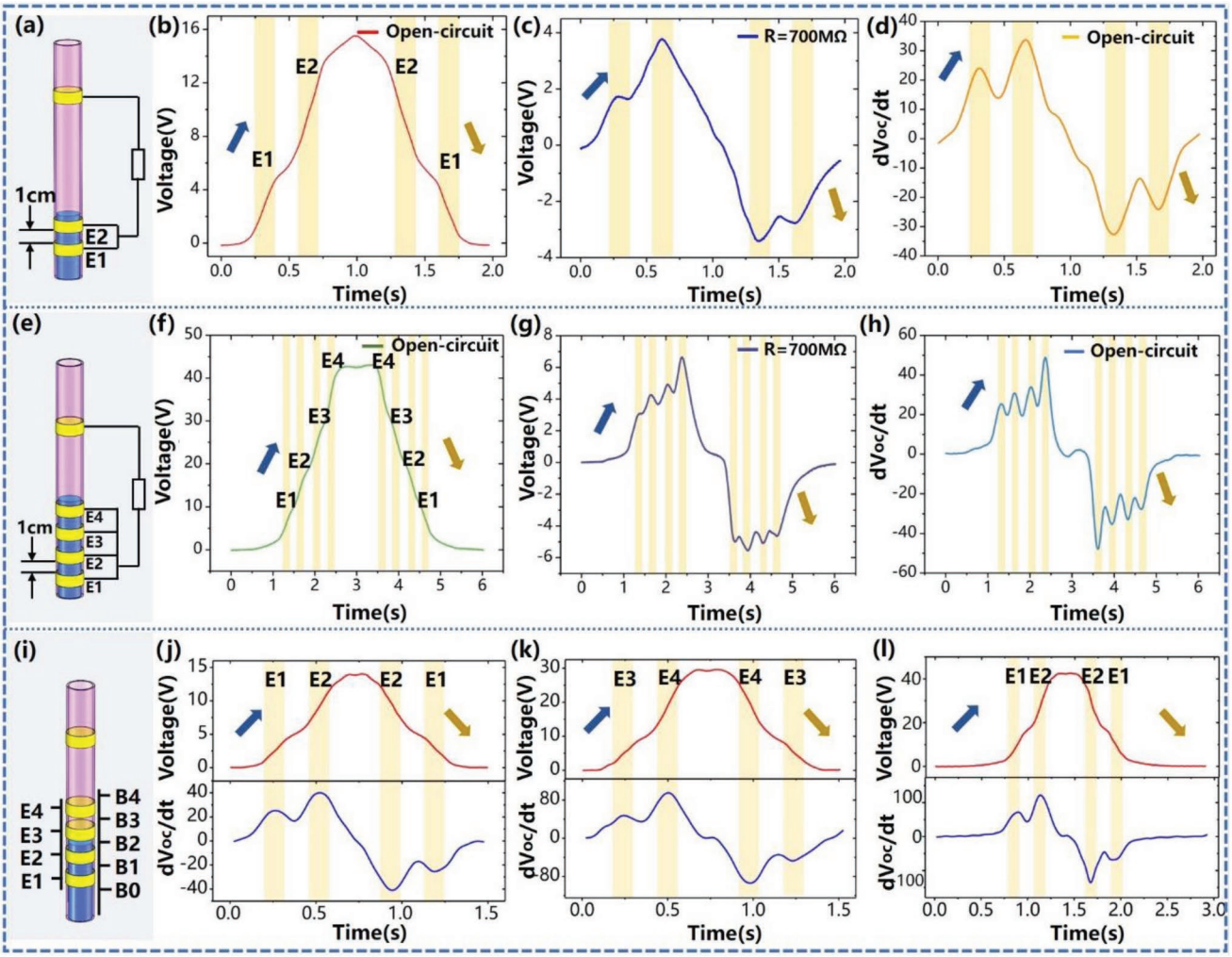

Figure 3. The electrical performance of the LST-TENG with multiple bottom electrodes. a) The diagram of an LST-TENG with a pair of bottom electrodes. b) The open-circuit voltage, c) the voltage across a resistance of 700 MΩ, and d) the derivative of open-circuit voltage with respect to time during the water level rising above the electrode **E2** and falling below the electrode **E1.** e) The diagram of an LST-TENG with four bottom electrodes. f) The open-circuit voltage, g) the voltage between a resistance of 700 MΩ, and h) the differentiating signals of the open-circuit voltage output during the water level rising above the electrode **E4** and falling below the electrode **E1**. i) The diagram of an LST-TENG with marks of multiple electrodes and blank regions. The output voltage and the dV_{OC}/dt of the LST-TENG when the water increases from j) the **B0** to **B2**, and k) the **B2** to **B4**. l) The output voltage and the dV_{OC}/dt of the LST-TENG when the water level increases from **B0** to **B2** with the **B0** height of 5 cm.

respectively. The height of the blank region and electrode is both 10 mm. Similar to the observation of V_{OC} in Figure 2c(i), the open-circuit voltage varies faster within the electrode region than that in the blank region (Figure 3b). However, when the water level increases from **E1** and **E2**, the maximum value of the open-circuit voltage of the LST-TENG with the blank region height of 10 mm is around 15 V, which is smaller than that of the LST-TENG with the blank region height of 50 mm. The main effect might be due to the larger capacitance with smaller blank region. Correspondingly, the induced voltage V_{OC_b} for the smaller blank region becomes lower. According to Equation (2), the total V_{OC} would also decreases. The smaller height of the blank region further results in a disturbed short-circuit current signal, as shown in Figure S2 of the Supporting Information. This suggests that it is not proper to utilize the current signal to identify the smaller scale water level for the LST-TENG.

Compared to the current signal (Figure S2, Supporting Information) and the voltage across a resistance of 700 MΩ (Figure 3c), it is found that the derivative of voltage with respect to time could be served as a robust and sensitive indicator to identify the water level (Figure 3d). There is an obvious positive peak/negative valley in the electrode region when water increases/decreases, as shown in Figure 3d. This phenomenon is also valid for the LST-TENG with multiple bottom electrodes (Figure 3e–h). Multiple peaks and valleys are observed in differentiating signals of the open-circuit voltage for water level rising above the fourth electrode **E4** (Figure 3h). Such phenomenon is due to that the V_{OC} of the LST-TENG increases/decreases faster as water rising/falling within the electrode region, while it increases/decreases slowly as water rising/falling within the blank region. Therefore, those peaks and valleys from the singles of dV_{OC}/dt can be used to identify the water level.

Furthermore, the effect of the initial water level on the output performance of the LST-TENG is also investigated. Figure 3j,k shows the output voltage and the dV_{OC}/dt of the LST-TENG when the water level rises from the **B0** to **B2**, and the **B2** to **B4**, respectively. Although the water displacement remains same for the two cases, it is interesting to find that the maximum value of V_{OC} is bigger for the higher initial water level. The main effect might be due to a larger internal capacitance because of a smaller blank area. Additionally, Figure 3l shows the output voltage of the LST-TENG when the water level increases from **B0** to **B2** with the **B0** height of 5 cm. It is also found that the maximum value of V_{OC} is bigger for the longer water displacement. However, as shown in Figure 3j–l, these positions of peaks and valleys from the singles of dV_{OC}/dt are in accordance with the distribution of bottom electrodes for all cases.

To further test the robustness of the LST-TENG for water level detecting, the performance of the LST-TENG in different salinity seawater and variable frequency is investigated. **Figure 4**a shows the output voltage peak of the LST-TENG at the salinity of 0–35 mg mL^{-1}. It is found that the peak value of the output voltage at the same water level decays exponentially with increasing salinity. For example, the V_{OC} of the WS-TENG at the water level of 70 mm exponentially decreases from 40 to 7 V as salinity increasing from 0 to 35 mg mL^{-1}. This supports that high ions' concentration reduces induced charges

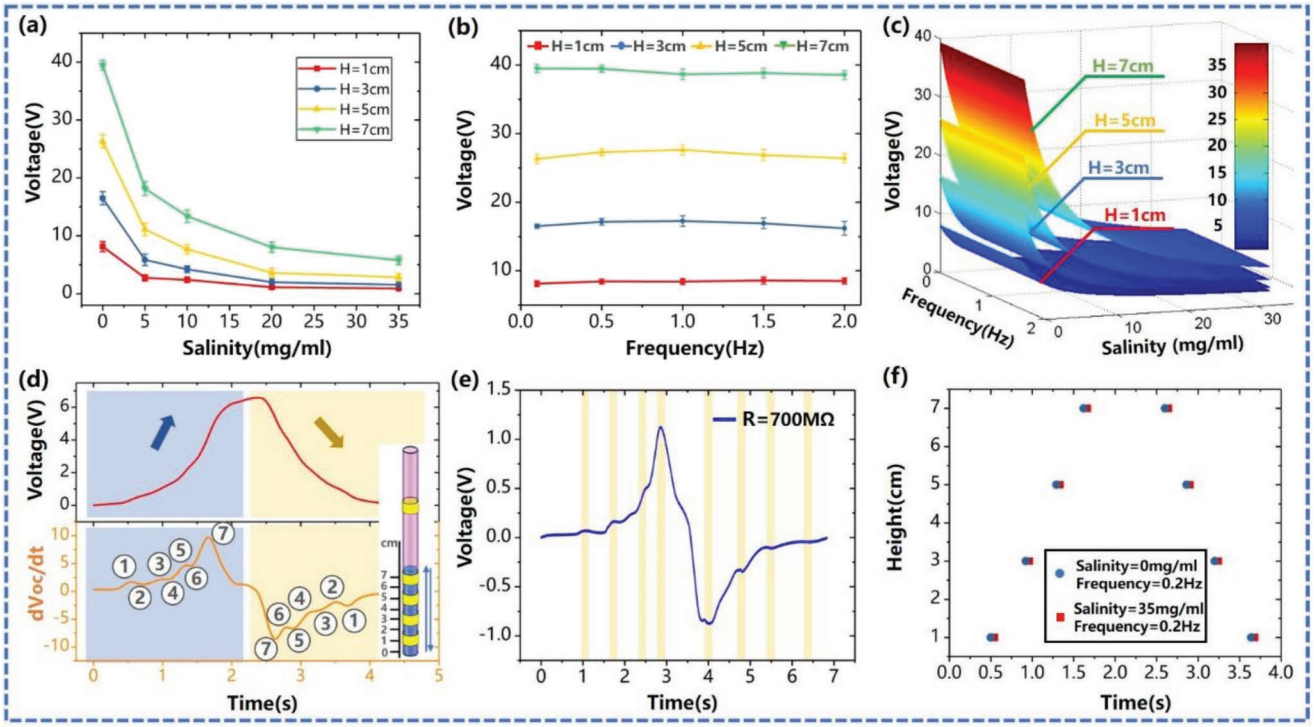

Figure 4. Effect of salinity and frequency on the performance of the LST-TENG. a) The output voltage peak of the LST-TENG at different salinity water. b) The output voltage peak of the LST-TENG at different frequency. c) A 3D graph of the output voltage peak at different salinity and frequency. d) The characteristics of output voltage signals and its differentiating signals and e) the load voltage of the LST-TENG for the salinity of 35 mg mL^{-1}. f) The instantaneous water level detected according to the peaks and valleys of dV_{OC}/dt for the salinity of 35 mg mL^{-1}.

in electrodes, thus resulting in the decrease of the output voltage.[40,41] Therefore, the output open-circuit voltage peak is not a suitable choice for detecting water level, as it is highly dependent on water salinity. By comparison, the step-like variation of V_{OC} and the peaks and valleys of dV_{OC}/dt are also observed at different salinity, as shown in Figure 4d. Then the water level H can be successfully determined with the accuracy of 10 mm (Figure 4f), which is the height of electrode region and blank region. The positions of peaks and valleys of dV_{OC}/dt at the salinity of 35 mg mL^{-1} are the same with those at pure water. Thus, the instantaneous water level H can be detected according to the peaks and valleys of dV_{OC}/dt for both the salinity of 35 mg mL^{-1} and pure water (Figure 4f). This suggests that the present method for detecting water level is robust.

The peaks of output voltage of the LST-TENG under the frequency between 0.2–2 Hz are shown in Figure 4b. The variable frequency of water level is precisely controlled by a linear motor. Obviously, the output voltage peaks are independent of the variable frequency. This is consistent with Equation (S5) of the Supporting Information, which indicates that V_{OC} depends on water level, and is independent of frequency. This is further supported by a 3D graph of the output voltage peak under different salinity and frequency, as shown in Figure 4c.

In addition, the electrical output of the LST-TENG with four distributed electrodes was investigated as the water level varying in the range of 0–70 mm at the frequency of 0.2 Hz. By using different resistors as external loads, the power output of the LST-TENG was measured (Figure S2a, Supporting Information). It is found that the output voltage increases quickly as the resistance increases from 0.1 to 5000 MΩ, and then saturates when the resistance is further increased. As a result, the output power density is maximized at 0.6 μW with a load resistance of 500 MΩ. Furthermore, Figure S2b of the Supporting Information shows the charging voltage as a function of the charging time by using a commercial capacitor of 5 μF. This suggests that the LST-TENG could also harvest energy from liquid–solid contact.

2.3. Demonstration

The application of LST-TENG as a water level sensor for ship draft detecting is shown in **Figure 5** and Video S1 (Supporting Information). An LST-TENG with four distributed electrodes is installed onto the surface of a semi-submersible ship model Figure 5a. Both the height of the electrode and the blank region are 10 mm each. Therefore, the accuracy of the water level sensor is 10 mm, which can be further improved by utilizing narrower electrodes with closer distribution. As shown in Figure S3 of the Supporting Information, an LST-TENG with both the electrode and blank region width of 5 mm could identify the water level with the accuracy of 5 mm. It is also worth noting that, at present, the drafts are mainly measured with a "banded" scale. The bottom of each draft mark is the draft in

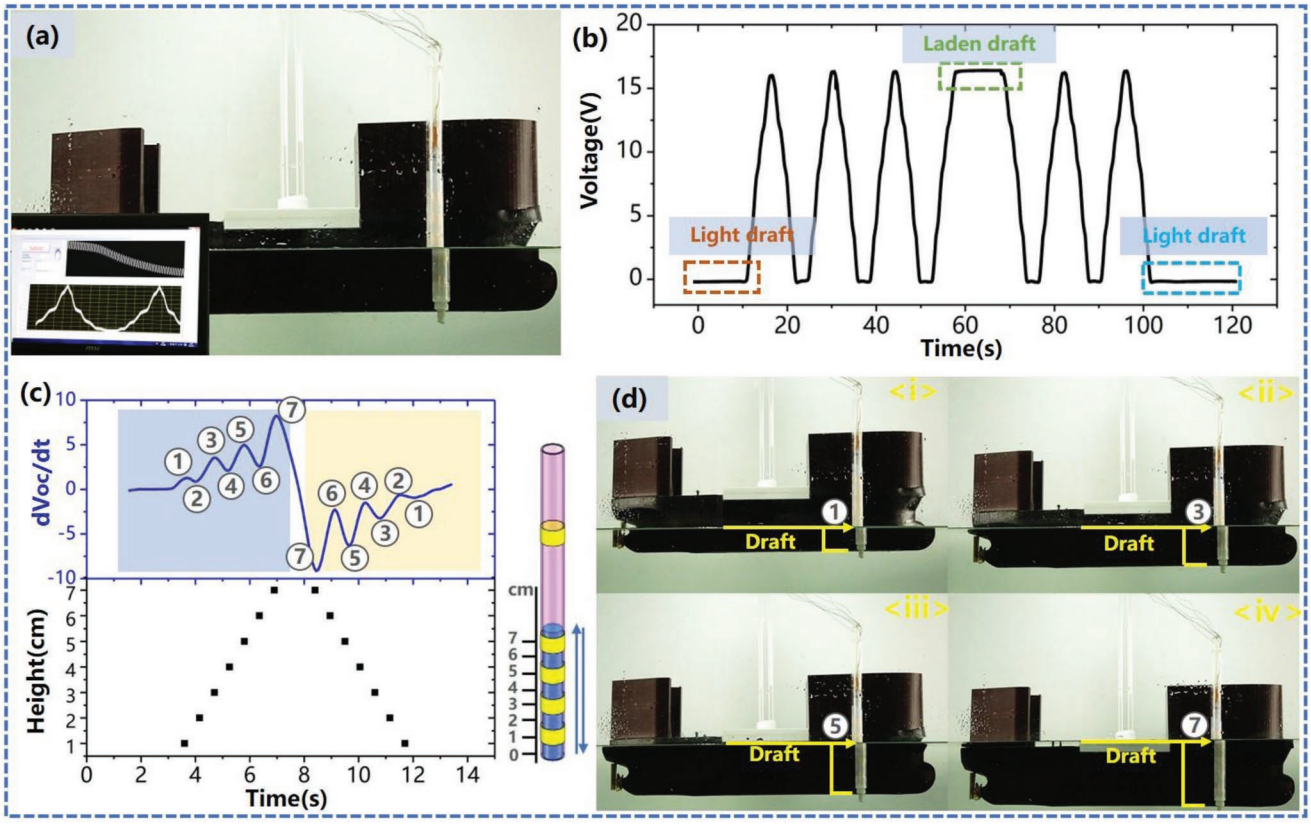

Figure 5. The application of LST-TENG as a water level sensor for ship draft detecting. a) Image of the LST-TENG installed onto a ship. b) The output voltage of the LST-TENG during the cargo loading and unloading of the ship. c) The dV_{OC}/dt signals of LST-TENG and detected water level during the cargo loading and unloading of the ship. d) Images of the ship at different water level.

decimeters and each mark is one decimeter high. Therefore, the accuracy of the LST-TENG is around ten times higher than that of the traditional draft mark on the ship. The LST-TENG is placed into an acrylic tube with a larger diameter. The air gap between the PTFE tube and the acrylic tube can reduce the effect of shielding from the water. The ship is able to rise or fall in water by controlling the shaft of a linear motor. Correspondingly, it is similar to the variation of the water level during the cargo loading and unloading of the ship. Figure 5b shows the output voltage of the LST-TENG at different water level.

It is found that the voltage increases from 0 to 16 V when the ship is gradually loaded from light draft to laden draft. Here, the light draft refers to the level that water reaches on a ship when it is not carrying anything. The laden draft is the depth of a ship when it is carrying something such as cargo, passengers, fuel, water, stores, dunnage, and such other items necessary for use on a voyage. It is worth noting that the voltage remains stable when the ship is in laden draft. The performance of the LST-TENG is further investigated when the water level suddenly stops at a specific position (Figure S4, Supporting Information). The voltage is kept steady during the water level stopping at the blank region or electrode region, then it would increase when the water level keeps rising. Correspondingly, it is found that the value of dV_{OC}/dt is nearly constant zero when the water level stops at a specific position. A step-like variation during the cargo loading and unloading of the ship is also observed in Figure 5b. The peaks and valleys are obviously observed in the dV_{OC}/dt signals, thus the water level is detected (Figure 5c). The images of the ship at different draft of 1, 3, 5, and 7 cm, are shown in Figure 5d(i–iv). The peaks of dV_{OC}/dt corresponding to the ship draft are marked in the diagrams. Furthermore, considering the unit of ship draft is meter, we have fabricated a longer sensor with 1.2 m long and 20 bottom electrodes uniformly distributed along the PTFE tube (Figure S5, Supporting Information). It can also be used to identify the water level. In addition. the durability test of the LST-TENG shows that the output voltage peak remains stable after 2000 cycles at the frequency of 0.9 Hz (Figure S6, Supporting Information). The LST-TENG show great reliability as a robust water level sensor.

3. Conclusion

In summary, a self-powered water level sensor based on LST-TENG is proposed and analyzed. The LST-TENG is made of multiple copper electrodes uniformly distributed along a PTFE tube. The working principle of the LST-TENG was systematically investigated by experimental results and finite-element simulations. When water rises/falls inside the tube, the output voltage between the top main electrode and other distributed electrodes is induced by the liquid–solid contact electrification. The open-circuit voltage of LST-TENG varies faster when water flows within the electrode region than the blank region. Thus, it is found that the obvious peaks in the derivative of open-circuit voltage with respect to time are in correspondence with electrode distribution. Then it could be utilized as a robust and sensitive indicator for detecting the water level as the number of obvious peaks in the derivative of open-circuit voltage is directly related to the water level height. In addition, the output power density of the LST-TENG is maximized at 0.6 μW with a load resistance of 500 MΩ. In a water tank, the ship dynamic draft is successfully detected using the LST-TENG with the accuracy of 10 mm, which is ten times higher than the traditional draft mark on the ship. The LST-TENG shows great reliability as a robust and accurate water level sensor.

4. Experimental Section

Fabrication of the LST-TENG: The fabrication of the LST-TENG is shown in Figure S4 of the Supporting Information. For the PTFE tube with an outer diameter of 17 mm and an inner diameter of 15 mm. The copper electrodes with the height of 10 mm are uniformly distributed along the PTFE tube. In the demonstration experiment, the prepared LST-TENG was placed in an acrylic tube with a diameter of 20 mm. The air gap between the PTFE tube and the water can reduce the effect of shielding from the water.

Measurement of the Fabricated Devices: The internal surface nanostructure of the PTFE tube was characterized by field emission scanning electron microscope (SU-8010, Hitachi). The main electrode and the distributed electrodes were connected to the Keithley 6514 electrometer to measure the output voltage. As shown in Figure 3a, the system mainly consists of a linear motor (LinMot E1100), a syringe, an LST-TENG and a water tank. A linear motor is vertically fixed above the water tank. The top of the linear motor output shaft is connected with the needle push rod of the syringe. The needle part of the syringe is connected with the top of the PTFE tube. The bottom of the tube is immersed into the water tank. The syringe can be sucked and drained by controlling the linear motor to reciprocate at a constant speed. Therefore, water level would change as water rises and falls in the tube. The motion equation of the linear motor is realized by setting its stroke, speed, and acceleration in a LabVIEW code.

Supporting Information

Supporting Information is available from the Wiley Online Library or from the author.

Acknowledgements

X.Z., M.Y., and Z.M. contributed equally to this work. The authors are grateful for the support received from the National Key Research and Development Program of China (Nos. 2016YFA0202703 and 2016YFA0202704), the National Natural Science Foundation of China (Nos. 51879022, 51506019, 61875015, 31571006, and 21801019), the Young Elite Scientists Sponsorship Program by CAST (2016QNRC001), the Beijing Natural Science Foundation (2182091), and the National Youth Talent Support Program.

Conflict of Interest

The authors declare no conflict of interest.

Keywords

liquid–solid contact electrification, marine sensor, ship draft detecting, triboelectric nanogenerator, water level sensor

Received: January 11, 2019
Revised: February 22, 2019
Published online:

[1] L. Xinli, C. Xianqiao, L. Huaihan, C. Xiumin, presented at 2015 International Conference on Transportation Information and Safety (ICTIS), Wuhan, China, 25–28 June **2015**.
[2] H. W. Gu, W. Zhang, W. H. Xu, Y. Li, *App. Mech. Mater.* **2013**, *333–335*, 312.
[3] H. Zheng, Y. Huang, Y. Ye, *IEEE Trans. Instrum. Meas.* **1999**, *48*, 1014.
[4] Z. L. Wang, L. Lin, J. Chen, S. Niu, Y. Zi, *Triboelectric Nanogenerators*, Springer, Berlin, Germany **2016**.
[5] Z. L. Wang, *Mater. Today* **2017**, *20*, 74.
[6] R. D. I. G. Dharmasena, K. D. G. I. Jayawardena, C. A. Mills, J. H. B. Deane, J. V. Anguita, R. A. Dorey, S. R. P. Silva, *Energy Environ. Sci.* **2017**, *10*, 1801.
[7] H. Ryu, J. H. Lee, U. Khan, S. S. Kwak, R. Hinchet, S.-W. Kim, *Energy Environ. Sci.* **2018**, *11*, 2057.
[8] H. Guo, X. Pu, J. Chen, Y. Meng, M.-H. Yeh, G. Liu, Q. Tang, B. Chen, D. Liu, S. Qi, C. Wu, C. Hu, J. Wang, Z. L. Wang, *Sci. Rob.* **2018**, *3*, eaat2516.
[9] S. L. Zhang, M. Xu, C. Zhang, Y.-C. Wang, H. Zou, X. He, Z. Wang, Z. L. Wang, *Nano Energy* **2018**, *48*, 421.
[10] M. Xu, P. Wang, Y.-C. Wang, S. L. Zhang, A. C. Wang, C. Zhang, Z. Wang, X. Pan, Z. L. Wang, *Adv. Energy Mater.* **2018**, *9*, 1702432.
[11] J. W. Lee, H. J. Cho, J. Chun, K. N. Kim, S. Kim, C. W. Ahn, I. W. Kim, J.-Y. Kim, S.-W. Kim, C. Yang, J. M. Baik, *Sci. Adv.* **2017**, *3*, e1602902.
[12] G. Suo, Y. Yu, Z. Zhang, S. Wang, P. Zhao, J. Li, X. Wang, *ACS Appl. Mater. Interfaces* **2016**, *8*, 34335.
[13] M. Perez, S. Boisseau, M. Geisler, G. Despesse, J. L. Reboud, *J. Phys.: Conf. Ser.* **2016**, *773*, 012021.
[14] J. Chun, B. U. Ye, J. W. Lee, D. Choi, C.-Y. Kang, S.-W. Kim, Z. L. Wang, J. M. Baik, *Nat. Commun.* **2016**, *7*, 12985.
[15] J. Kim, J. H. Lee, H. Ryu, J.-H. Lee, U. Khan, H. Kim, S. S. Kwak, S.-W. Kim, *Adv. Funct. Mater.* **2017**, *27*, 1700702.
[16] M. Xu, T. Zhao, C. Wang, S. L. Zhang, Z. Li, X. Pan, Z. L. Wang, *ACS Nano* **2019**, *13*, 1932.
[17] C. Hao, J. He, C. Zhai, W. Jia, L. Song, J. Cho, X. Chou, C. Xue, *Nano Energy* **2019**, *58*, 147.
[18] Y. Wu, Y. Su, J. Bai, G. Zhu, X. Zhang, Z. Li, Y. Xiang, J. Shi, *J. Nanomater.* **2016**, *2016*, 1.
[19] L. Pan, J. Wang, P. Wang, R. Gao, Y.-C. Wang, X. Zhang, J.-J. Zou, Z. L. Wang, *Nano Res.* **2018**, *11*, 4062.
[20] Z. Li, J. Chen, J. Zhou, L. Zheng, K. C. Pradel, X. Fan, H. Guo, Z. Wen, M. H. Yeh, C. Yu, *Nano Energy* **2016**, *22*, 548.
[21] H. Ouyang, J. Tian, G. Sun, Y. Zou, Z. Liu, H. Li, L. Zhao, B. Shi, Y. Fan, Y. Fan, Z. L. Wang, Z. Li, *Adv. Mater.* **2017**, *29*, 1703456.
[22] M. Shi, H. Wu, J. Zhang, M. Han, B. Meng, H. Zhang, *Nano Energy* **2017**, *32*, 479.
[23] Z. Liu, Y. Ma, H. Ouyang, B. Shi, N. Li, D. Jiang, F. Xie, D. Qu, Y. Zou, Y. Huang, H. Li, C. Zhao, P. Tan, M. Yu, Y. Fan, H. Zhang, Z. L. Wang, Z. Li, *Adv. Funct. Mater.* **2019**, *29*, 1807560.
[24] M. Xu, S. Wang, S. L. Zhang, W. Ding, P. T. Kien, C. Wang, Z. Li, X. Pan, Z. L. Wang, *Nano Energy* **2019**, *57*, 574.
[25] X. Zhang, Y. Zheng, D. Wang, F. Zhou, *Nano Energy* **2017**, *40*, 95.
[26] P. Bai, G. Zhu, Q. Jing, J. Yang, J. Chen, Y. Su, J. Ma, G. Zhang, Z. L. Wang, *Adv. Funct. Mater.* **2014**, *24*, 5807.
[27] H. Guo, J. Chen, M. H. Yeh, X. Fan, Z. Wen, Z. Li, C. Hu, Z. L. Wang, *ACS Nano* **2015**, *9*, 5577.
[28] J. Yang, J. Chen, Y. Su, Q. Jing, Z. Li, F. Yi, X. Wen, Z. Wang, Z. L. Wang, *Adv. Mater.* **2015**, *27*, 1316.
[29] D. Choi, D. W. Kim, D. Yoo, K. J. Cha, M. La, D. S. Kim, *Nano Energy* **2017**, *36*, 250.
[30] Q. Shi, H. Wu, H. Wang, H. Wu, C. Lee, *Adv. Energy Mater.* **2017**, *7*, 1701300.
[31] J.-G. Sun, T. N. Yang, I. S. Kuo, J.-M. Wu, C.-Y. Wang, L.-J. Chen, *Nano Energy* **2017**, *32*, 180.
[32] U. Khan, T. H. Kim, H. L. Kang, J. H. Lee, H. J. Yoon, R. Bhatia, I. Sameera, W. Seung, H. Ryu, C. Falconi, *Nano Energy* **2015**, *17*, 356.
[33] S. L. Zhang, Y.-C. Lai, X. He, R. Liu, Y. Zi, Z. L. Wang, *Adv. Funct. Mater.* **2017**, *27*, 1606695.
[34] D. Chaoran, T. Wei, L. Long, C. Baodong, L. Meicheng, W. Z. Lin, *Adv. Funct. Mater.* **2018**, *28*, 1801606.
[35] X. J. Zhao, J. J. Tian, S. Y. Kuang, H. Ouyang, L. Yan, Z. L. Wang, Z. Li, G. Zhu, *Adv. Mater. Interfaces* **2016**, *3*, 1600187.
[36] J. Tian, H. Feng, L. Yan, M. Yu, H. Ouyang, H. Li, W. Jiang, Y. Jin, G. Zhu, Z. Li, Z. L. Wang, *Nano Energy* **2017**, *36*, 241.
[37] Y. Su, G. Zhu, W. Yang, J. Yang, J. Chen, Q. Jing, Z. Wu, Y. Jiang, Z. L. Wang, *ACS Nano* **2014**, *8*, 3843.
[38] J. Chen, H. Guo, J. Zheng, Y. Huang, G. Liu, C. Hu, Z. L. Wang, *ACS Nano* **2016**, *10*, 8104.
[39] S. Wang, Y. Xie, S. Niu, L. Lin, Z. L. Wang, *Adv. Mater.* **2014**, *26*, 2818.
[40] L. Pan, J. Wang, P. Wang, R. Gao, Y.-C. Wang, X. Zhang, J.-J. Zou, Z. L. Wang, *Nano Res.* **2018**, *11*, 4062.
[41] C. Hughes, L.-H. Yeh, S. Qian, *J. Phys. Chem. C* **2013**, *117*, 9322.